gels

MDPI

Article

Fabrication of Cardanol Side-Chain Hydrophobically Associating Thermosensitive Gel System with Thermally Induced Network Evolution for Deep Fluid Diversion

Jianxun Meng [1,2], Xiangbin Liu [2,3], Qingsong Li [2,3], Zhixuan Zhu [2,3,*], Guoliang Mao [1,*], Qingguo Wang [2,3], Qi Zhou [2,3], Baize Zhu [2,3], Biao Zhang [2,3], Xuesong Lin [2,3] and Lichao Wang [2,3]

[1] College of Chemistry and Chemical Engineering, Northeast Petroleum University, Daqing 163318, China; mengjianxun@petrochina.com.cn
[2] Heilongjiang Provincial Key Laboratory of Oil and Gas Reservoir Stimulation, Daqing 163453, China; liuxiangbin@petrochina.com.cn (X.L.); liqingsong@petrochina.com.cn (Q.L.); wqg@petrochina.com.cn (Q.W.); zhouqi25@petrochina.com.cn (Q.Z.); baizezhu@petrochina.com.cn (B.Z.); zhangbiao22@mails.ucas.ac.cn (B.Z.); linxuesong@petrochina.com.cn (X.L.); wanglichao_cyy@petrochina.com.cn (L.W.)
[3] Daqing Oilfield Production Technology Institute, Daqing 163453, China
* Correspondence: petrozhuzx@163.com (Z.Z.); maoguoliang@nepu.edu.cn (G.M.)

Abstract

Conventional polymer gels for deep fluid diversion in moderate-temperature (40–60 °C) reservoirs are constrained by the chromatographic separation of crosslinkers and poor gelation controllability. In this work, a side-chain pendant decoupling molecular design strategy is proposed. Using cardanol glycidyl ether, diethylenetriamine (DETA), and polyethylene glycol diglycidyl ether (PEGO), a stepwise route exploits the differential reactivity of mono- versus di-epoxide groups to graft cardanol C15 alkyl chains as freely pendant side groups onto a PEGO/DETA covalent network. The covalent network provides a mechanical skeleton, while the pendant C15 chains act as independent thermoresponsive switches, liberating the C15 chains from topological constraints. This endows the hydrogel with a clear thermoresponsive transition around 40 °C, with G′ increasing to 980 Pa and the transmittance dropping from 28.9% to below 4%. Kinetic analysis indicated a transition from diffusion-controlled to chemically controlled network growth. The Avrami exponent n ranged from 0.85 to 1.28 across the tested temperatures. The poor linearity of the Arrhenius fits (R^2 = 0.62 and 0.35) indicates non-Arrhenius behavior, consistent with the proposed synergistic dual mechanism. Given the unavoidable salinity of formation water in actual reservoirs, the effect of salinity on gelation kinetics was further examined. At 45 °C, varying the NaCl concentration from 0 to 5000 mg/L affected gelation kinetics, while the measured plateau storage moduli remained similar under the investigated conditions. Physical simulation experiments showed a plugging rate of 96.1% at 60 °C in deionized water, and in situ gelation in the core under simulated reservoir brine led to a 99.98% permeability reduction within 60 min. This cardanol-derived hydrogel with engineered side chains establishes a molecular engineering principle in which pendant grafting liberates hydrophobic chains from topological constraints, offering a new paradigm for cardanol-derived intelligent oilfield chemicals in deep reservoir conformance control.

Keywords: cardanol; side-chain pendant; thermosensitive gel; hydrophobic association; gelation kinetics

Check for updates

Academic Editor: Jean-Michel Guenet

Received: 23 September 2026
Revised: 20 October 2026
Accepted: 23 October 2026
Published: 28 October 2026

Copyright: © 2026 by the authors. Licensee MDPI, Basel, Switzerland. This article is an open access article distributed under the terms and conditions of the Creative Commons Attribution (CC BY) license.

1. Introduction

Global oil and gas exploration has progressively extended toward deeper and more complex reservoirs [1]. Moderate-temperature (40–60 °C) reservoirs that have been developed for a long time have become major arenas for enhanced oil recovery (EOR) because of their substantial remaining reserves and active development potential [2,3]. However, such reservoirs commonly suffer from strong heterogeneity, and preferential flow channels have formed after long-term waterflooding [4]. Injected fluids have channeled through high-permeability pathways, while substantial remaining oil in low-permeability zones has remained unswept, which seriously restricts the ultimate recovery factor. Polymer gel systems have been widely recognized as one of the most important chemical means for deep fluid diversion [5]. They can form three-dimensional networks in situ within high-permeability channels, thereby reducing the permeability of these channels and diverting subsequent injected fluids into low-permeability zones. Among various gel systems, polyacrylamide-based gels have been widely applied because of their cost advantages and well-established crosslinking reactions [6]. However, these conventional systems, which rely on static chemical crosslinking by metal ions or organic crosslinkers, face two fundamental and coupled challenges during deep migration [7]. On the one hand, the chromatographic separation effect caused by differences in adsorption and migration velocity between polymers and crosslinkers in porous media has led to uncontrollable gelation fronts and nonuniform gel strength along the migration path [8]. On the other hand, moderate-temperature reservoirs have often been associated with saline formation water, in which divalent Ca^{2+} and Mg^{2+} ions compress the electrical double layer of polymer chains through electrostatic screening, inducing chain coiling and reducing the hydrodynamic radius [9]. These ions also competitively coordinate with crosslinking sites, thereby weakening or even deactivating crosslinking reactivity. As a result of these two coupled limitations, the gelation time, gel strength, and plugging location of conventional gels have been difficult to predict and guarantee. These bottlenecks have driven the emergence of the concept of smart gels, with the core aim of enabling materials to sense and actively adapt to reservoir conditions. Among various environmental response mechanisms, temperature-triggered gels have been regarded as one of the most engineered and feasible technical routes because their triggering signal occurs naturally in formations and requires no external chemical trigger. Since Tanaka first reported the volume phase transition of poly(N-isopropylacrylamide), fundamental research on thermoresponsive polymer materials has made considerable progress [10,11]. However, early achievements in this field mostly focused on biomedical applications [12]. Meanwhile, the phase transition temperatures of such gels are usually designed within the physiological range of 30–37 °C, and their mechanical strength and long-term thermal stability are far from sufficient for downhole conditions. Harsh reservoir conditions have driven the development of various temperature-resistant polymer gels and microsphere systems [13,14]. However, these systems are primarily designed for reservoirs above 80 °C or even 120 °C, and their crosslinking kinetics and long-term stability are often suboptimal in the 40–60 °C range. Consequently, existing technical systems show a clear temperature mismatch in this moderate-temperature window. Biomedical thermosensitive gels are unsuitable for reservoir use because their transition temperatures and mechanical strength are designed for physiological conditions. In contrast, high-strength temperature-resistant gels rely on crosslinking or reinforcement mechanisms that require higher temperatures to be fully activated, and thus often struggle to achieve comparable strength within the 40–60 °C range [15,16]. Therefore, the development of a smart gel capable of precisely adapting to moderate-temperature reservoir conditions while combining rapid response with high strength is a clear and urgent research direction in oilfield chemistry [17].

Achieving the above objectives critically depends on precise molecular engineering of the crosslinked structure within the gel network. Hydrophobically associating polymer gel systems have received increasing attention because of their unique physical crosslinking mechanism in recent years [18]. Hydrophobically associating polymers are constructed by introducing a small number of hydrophobic groups onto hydrophilic backbones. In aqueous solutions, these hydrophobic groups spontaneously aggregate into dynamic physically crosslinked networks, which exhibit reversibility and self-healing characteristics and effectively enhance the shear resistance and environmental adaptability of gels. Existing studies have shown that hydrophobically modified preformed particle gels can reduce water phase permeability by a factor of 6–12, showing promising potential for deep fluid diversion [18]. Thermally associating polymers have further incorporated thermoresponsive characteristics into hydrophobically associating systems. The hydrophobic groups in these polymers remain hydrophilic at low temperatures and become hydrophobic and associate with one another to form three-dimensional networks once the temperature rises above a threshold [19]. This process is temperature-responsive. Such systems have provided an ideal molecular basis for temperature-controlled in situ gelation. The source and molecular structure of hydrophobic functional monomers have directly determined the strength of association behavior and response characteristics; meanwhile, the use of renewable biomass resources to develop eco-friendly oilfield chemicals has become an important trend [20]. Therefore, finding hydrophobic units that combine the advantages of natural sources with efficient association ability has become an important direction in this field. Cardanol, a natural phenolic compound derived from cashew nut shell liquid, has stood out because of its unique molecular structure, low cost, and high availability. Its structure contains a phenolic hydroxyl group, an aromatic ring, and a long C15 alkyl side chain [21,22]. A glucose-triazole-hydrogenated cardanol supramolecular gel has been prepared by coupling hydrogenated cardanol with glucose through a triazole linker [23]. This gel can exhibit stable temperature-responsive gelation in a water–methanol mixed solvent at an ultralow concentration of 0.03% weight per volume, as reported by Surya Prakash Rao et al. Cardanol polyoxyethylene ether has been synthesized from natural cardanol and has exhibited good interfacial activity and temperature and salt tolerance, reducing the oil–water interfacial tension to approximately 10^{-1} mN/m [24]. Fmoc-cardanol compounds have also been self-assembled into hydrogels. These studies have collectively indicated that the C15 long alkyl chain of cardanol has a natural structural advantage as a thermoresponsive module.

Previous studies have established the potential of hydrophobic association and cardanol modification for gel formation and reservoir conformance control. For example, hydrophobically modified acrylamide hydrogels have been investigated as preformed particle gels, using associative interactions to develop networks for permeability reduction. In another approach, cardanol has been incorporated into phenolic resin crosslinkers to prepare polymer gels with demonstrated dynamic gel-forming and plugging capabilities [25]. These approaches provide important precedents while differing in the molecular role assigned to the hydrophobic component and the route used to construct the gel network. The present study explores a pendant cardanol architecture constructed through stepwise epoxy–amine reactions. Monofunctional cardanol glycidyl ether introduces cardanol moieties onto DETA-derived units, whereas bifunctional PEGO participates in subsequent covalent network formation. This design combines a covalent supporting network with pendant hydrophobic groups intended to contribute temperature-dependent associative reinforcement. Its distinctive feature is the functional organization of network support and thermal response within the same material, rather than pendant hydrophobic substitution alone. The resulting structure–response relationship and plugging performance are examined under the selected moderate-temperature and simulated reservoir-brine conditions.

In this work, a side-chain pendant decoupling molecular design strategy was proposed and validated. Using cardanol glycidyl ether, diethylenetriamine (DETA), and polyethylene glycol diglycidyl ether (PEGO), a stepwise route exploits the differential reactivity of mono- versus di-epoxide groups to graft cardanol C15 alkyl chains as freely pendant side groups onto a PEGO/DETA covalent network. The chemical structure and the micromorphology of the cardanol side-chain gel were characterized. A block in Daqing Oilfield (60 °C, 5014 mg/L) was selected as the target reservoir, then the thermosensitive phase transition behavior and rheological mutation were investigated by ultraviolet-visible spectrophotometry and rotational rheometry. The temperature-driven transition in network growth dimension was quantitatively revealed through Avrami kinetic analysis combined with Arrhenius equation fitting, and the effect of salinity on the gelation process of the hydrogel system was further examined. Based on the above thermoresponsive and salinity-stable characteristics, the plugging performance at different temperatures was then evaluated. The proposed molecular design offers a basis for further development of thermoresponsive gels, while its applicability beyond the investigated temperature and salinity conditions requires additional validation. The resulting cardanol-derived hydrogel also shows promise for deep fluid diversion in moderate-temperature reservoirs, exhibiting temperature-dependent rheological strengthening and high plugging efficiency under the tested simulated formation-brine conditions.

2. Results and Discussion

2.1. Chemical Structure and Microscopic Morphology Characterization

The chemical structure and microscopic morphology of the prepared cardanol glycidyl ether and the prepolymer were systematically characterized, confirming the successful construction of the gel from the molecular to the microscopic scale and providing an understanding of its structural basis. Fourier transform infrared (FT-IR) spectroscopy and proton nuclear magnetic resonance (^{1}H NMR) analyses jointly confirmed the expected chemical reactions and structures. As shown in Figure 1A, the FT-IR spectrum of cardanol glycidyl ether exhibited a distinct epoxy group characteristic absorption band at 910 cm^{-1}; in the spectrum of the prepolymer obtained after reaction with diethylenetriamine (Figure 1B), this peak intensity decreased markedly, while a broad and strong absorption band appeared in the range of 3200–3500 cm^{-1}, attributed to the stretching vibrations of secondary amines and hydroxyl groups generated by the ring-opening reaction. The ^{1}H NMR spectra (Figure 2) provided finer evidence. The characteristic signals of epoxy protons (δ = 2.5–3.2 ppm) in the prepolymer spectrum essentially disappeared, with only trace residual signals corresponding to an epoxy conversion of 96.2%. New signals appeared in the δ = 3.3–3.8 ppm region, corresponding to the protons of the –CH(OH)–CH$_2$–N– structural units. Meanwhile, the characteristic signals of the benzene ring and long alkyl chain of cardanol were retained. These results confirmed the successful ring-opening addition between amine and epoxy groups. The hydrophobic cardanol units were covalently grafted onto the polymer backbone. These spectral data confirmed the successful synthesis of the prepolymer. More importantly, they revealed a key molecular structural feature of the gel system. The cardanol hydrophobic units were grafted as side groups onto the polymer backbone rather than embedded in the main chain. The formation of this pendant side-group structure originated from the chemoselectivity of the stepwise synthesis route. CGE is a mono-epoxy monomer and undergoes ring-opening addition with only one primary amine of DETA at low temperature. After the reaction, the epoxy group was completely consumed. The C15 long alkyl chain of cardanol thus becomes a side group pendant on the DETA unit. The subsequently added PEGO acted as a diepoxy crosslinker, whose two epoxy groups react with the remaining primary and secondary amines on different DETA units, achieving

interchain extension and network crosslinking. Since all epoxy groups of CGE are consumed in the prepolymerisation stage, the cardanol side groups do not participate in any further covalent bond formation during the entire gelation process. This structural feature indicates that the C15 alkyl chains of cardanol were present as freely pendant side groups from the very beginning of polymer backbone formation. Their thermally induced conformational changes and hydrophobic association behavior were not constrained by covalent crosslinking sites, providing molecular-level structural assurance for the gel to achieve a sensitive thermoresponsive response in the moderate-temperature range. Quantitative ^{1}H NMR analysis confirmed the nearly complete consumption of the epoxy groups in CGE and the preferential reaction with primary amines. Because the mono-epoxy CGE cannot form a second covalent bond after ring-opening, the cardanol C15 chains are structurally confined to remain as single-point, dangling side groups during subsequent PEGO crosslinking. Specifically, the integration results revealed an epoxy conversion of 96.2% and an average of 0.48 grafted cardanol units per DETA molecule, consistent with the feed molar ratio CGE:DETA = 1:2. The molar ratio of reacted primary to secondary amines was 9:1, confirming that CGE preferentially reacts with primary amines, leaving most secondary amine sites for subsequent crosslinking. Based on the feed stoichiometry (DETA:CGE = 2:1 and amine:epoxy = 1:1), the network contains approximately 1 C15 chain per 4.5 PEGO chains, with a cardanol content of 9.9 wt% in the dry network (corresponding to 8.4 wt% C15 phenol residue). Due to the highly swollen state of the gel (ESR = 21.2 g/g at 25 °C), the Flory–Rehner equation is highly sensitive to small uncertainties in the interaction parameter χ, and the dual-network architecture violates the assumption of a single-component affine network with permanent crosslinks. Therefore, a reliable calculation of the molecular weight between crosslinks (Mc) via Flory–Rehner theory is not meaningful. To provide a more precise formulation-based calculation for the cardanol-derived content, considering the batch size (0.02 mol DETA and 0.01 mol CGE) and the 20 wt% casting protocol, the cardanol incorporated into the dry network is 3.04 g per batch. This corresponds to 9.1–10.6 wt% of the dry network and 1.8–2.1 wt% of the hydrated hydrogel. The pendant C15 density is 0.30–0.35 mmol per gram of network, with a refined C15:PEGO molar ratio of 1:4.5. Because DETA and PEGO are petrochemical derivatives, this hydrogel is not fully bio-based. Based on feed stoichiometry, the bio-derived C15 phenol residue accounts for approximately 8.4 wt% of the dry network. While the C15 side chains originate from a biodegradable lipid backbone, the cross-linked hydrogel as a whole is not claimed to be biodegradable due to the covalent network [26]. The estimated raw-material cost of the formulation is approximately 0.6–0.8 USD/kg, comparable to or lower than anionic polyacrylamide. Meanwhile, the complete retention of the characteristic signals of the cardanol benzene ring and long alkyl chains in the FT-IR and NMR spectra confirmed that the hydrophobic side chains did not undergo degradation or side reactions during bulk polymerization.

This chemical structural design, particularly the freely pendant state of the cardanol side groups, directly determines the micromorphology and response behavior of the material. Scanning electron microscopy (SEM) observation of the sample revealed a typical porous three-dimensional network structure, as shown in Figure 3. Pore-size statistics further reveal a hierarchical structure in the freeze-dried gel. A dominant micropore population of 3–15 μm is observed within the network walls, accompanied by larger interdomain cavities of 20–120 μm between microphase-separated domains (Figure S1). Since SEM was performed on freeze-dried samples, the pore dimensions differ from those in the hydrated state, and the comparison with reservoir pore throats is therefore semiquantitative. This uniform and interconnected porous structure originates from microphase separation between the hydrophobic side groups of cardanol segments and the hydrophilic main chains of PEG segments during crosslinking. The hydrophobic side groups aggregate into

dynamic, physically crosslinked microdomains due to thermodynamic incompatibility. The hydrophilic chains form a continuous skeleton through covalent crosslinking by DETA and PEGO. The hydrophobic microdomains and the hydrophilic covalent skeleton combine to form a stable hybrid network with both physical and chemical crosslinks. The continuous and intact covalent skeleton endows the gel with the necessary mechanical strength, while the appropriate pore structure ensures its ability to interact with the surrounding water or formation fluids [27]. The physical association sites provided by the pendant side groups ensure its sensitive response to external temperature stimuli.

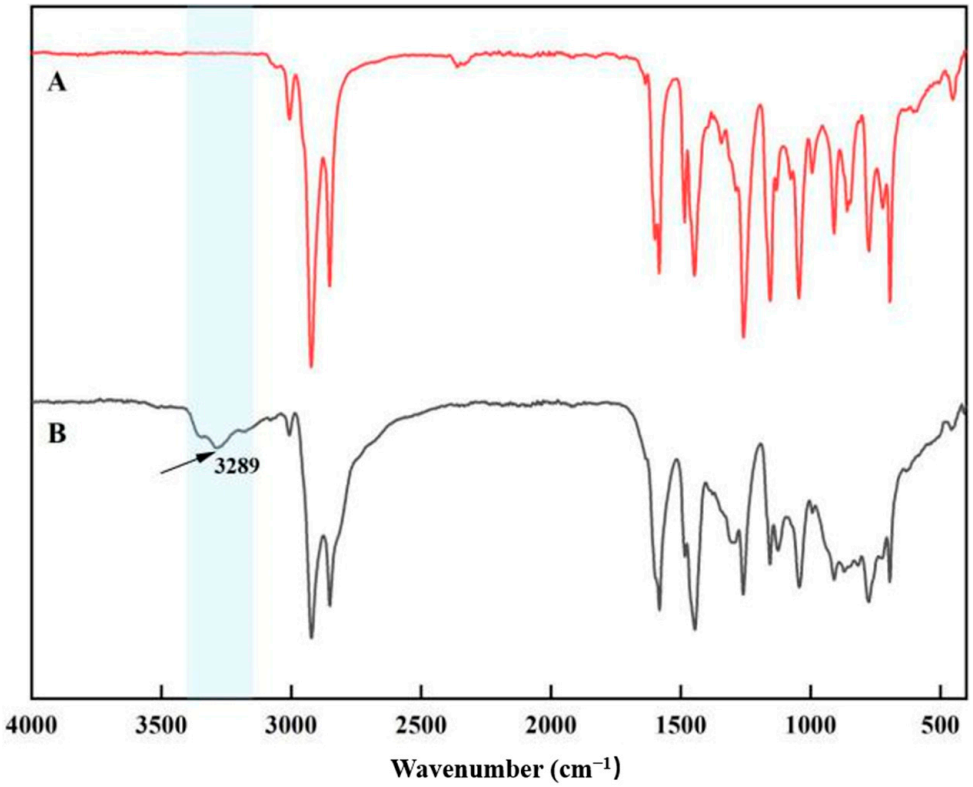
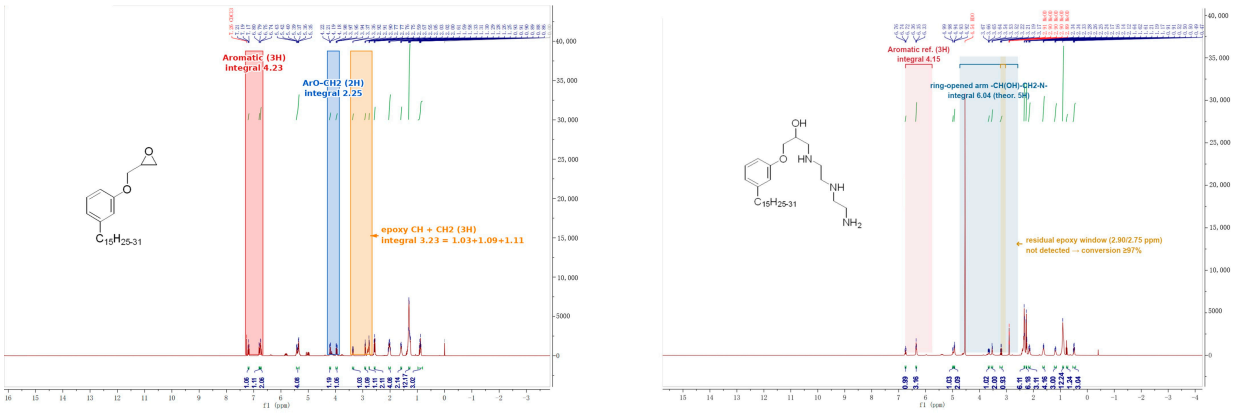
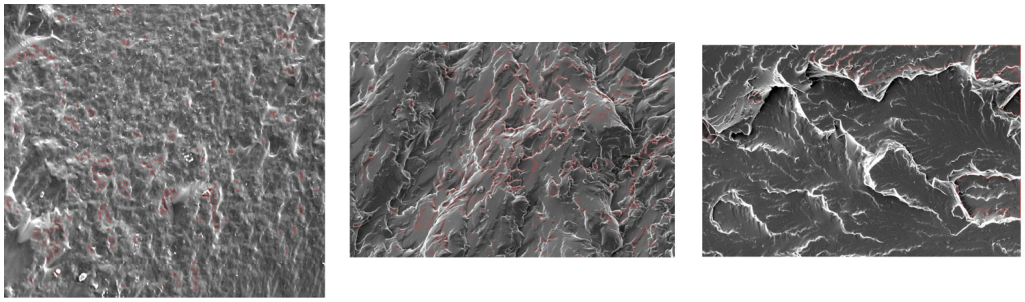


Figure 1. FT-IR spectra (**A**) CGE (**B**) CGE-DETA prepolymer.



(**a**) CGE (**b**) CGE-DETA prepolymer

Figure 2. ^{1}H NMR spectra of CGE and CGE-DETA prepolymer.



(**a**) The porous network (**b**) Inter-domain cavities (**c**) The smooth dense layer

Figure 3. SEM images of gel morphology.

2.2. Thermosensitivity and Rheological Behavior

The thermosensitive characteristics of the gel system were first intuitively verified by turbidity changes. As shown in Figure 4, at 560 nm, the transmittance of the gel solution dropped sharply from 28.9% to below 4% with increasing temperature, and the solution changed from clear and transparent to turbid and milky, indicating the onset of microphase separation and macroscopic phase transition within the system. The precursor solution was a freely flowing liquid at room temperature and became a non-flowing elastic body after heating to 60 °C.

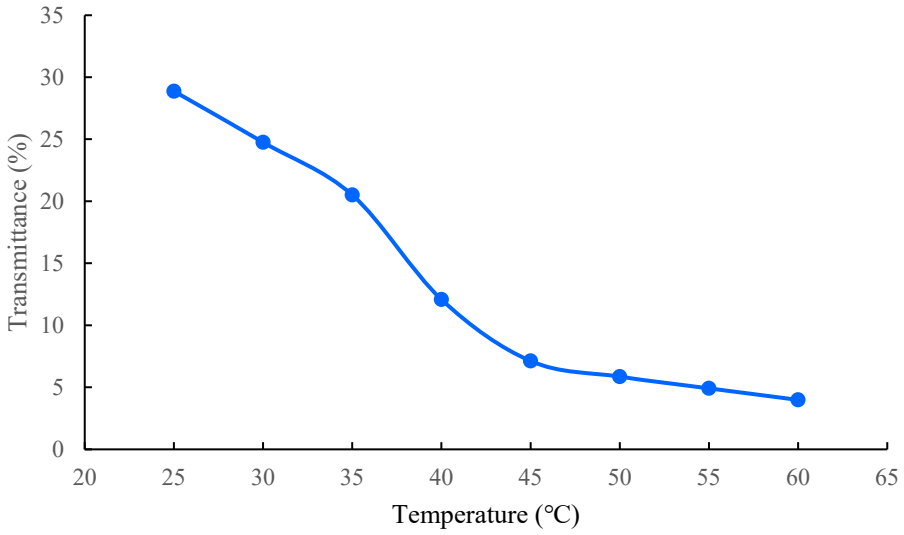
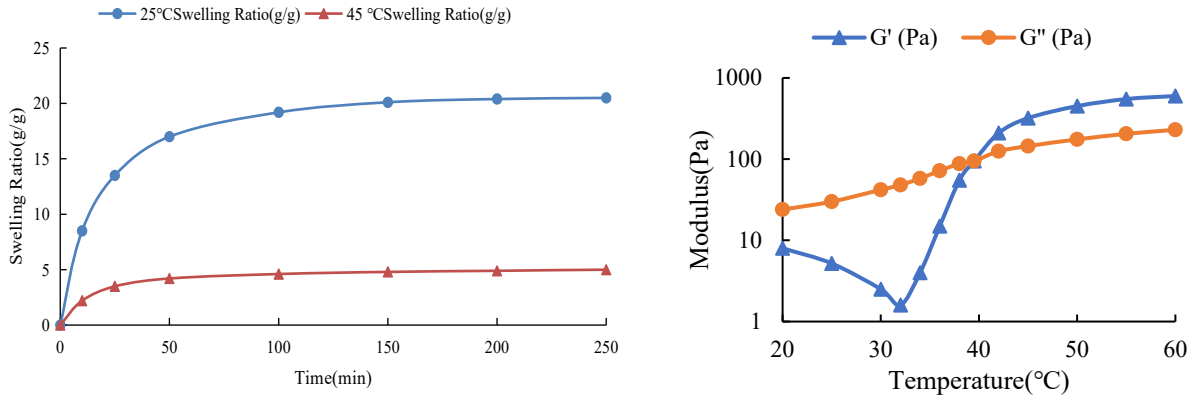


Figure 4. The UV transmittance curve of the cardanol-modified gel.

Swelling behavior further revealed the effect of the thermosensitive transition on the hydration state of the network. As shown in Figure 5a, at 25 °C, the dried gel exhibited typical hydrophilic network characteristics and absorbed water rapidly, reaching swelling equilibrium in approximately 6 h with an equilibrium swelling ratio (ESR) as high as 21.2 g/g. When the temperature increased to 45 °C, both the swelling rate and the ESR decreased significantly, and the ESR dropped sharply to 4.1 g/g. This drastic volume shrinkage resulted from the temperature-triggered hydrophobic association effect. Heating intensified the disruption of the hydration shell around the C15 long alkyl chains of cardanol, and hydrophobic interactions replaced hydrophilic interactions as the dominant driving force. The side chains spontaneously aggregated into dense, physically crosslinked microdomains to reach a more stable low-energy state and simultaneously expelled water molecules from the network, leading to overall dehydration and shrinkage of the gel. The results directly verified the effectiveness of the cardanol side chains as thermosensitive triggers. The pre-

ceding structural characterization confirmed that cardanol was pendant on the polymer backbone as side groups and was not locked by covalent bonds. Therefore, the C15 alkyl chains possessed sufficient conformational freedom and were able to sensitively complete the transition from extended hydration to collapsed aggregation under temperature stimulation. Had the cardanol units been embedded in the main chain or fixed at crosslinking points, their thermally induced motion would have been rigidly constrained by the covalent network, and such a large conformational change could not have been achieved.



(**a**) The curve of swelling rate over time (**b**) Rotational rheometer temperature sweep.

Figure 5. Thermosensitive behavior test results.

Temperature sweep measurements by rotational rheometry precisely captured the macroscopic mechanical transition corresponding to the phase transition (Figure 5b). At 25 °C, the loss modulus G″ was higher than the storage modulus G′, and the system behaved as a liquid sol. As the temperature increased, G′ began to increase significantly and crossed G″ at approximately 40 °C, which was identified as the gel point. G′ then increased rapidly and reached a plateau value of approximately 980 Pa at 45 °C, and the system transformed into a sturdy elastic gel. This rheological transition was highly consistent with the turbidity and swelling results. The overlap of the transition temperature ranges in these three measurements indicated that the thermosensitive transition was an intrinsic behavior of the system. Notably, the thermosensitive behavior of the gel originated from a purely physical association mechanism rather than a change in chemical crosslinking density. The chemical crosslinking network had already been fully formed during gel preparation at 45 °C for 48 h, and no new covalent bonds were generated during subsequent heating. Therefore, the increase in G′ with temperature was entirely attributed to the enhanced hydrophobic association of the cardanol side chains. The pendant C15 alkyl chains freely aggregated to form numerous dynamic physical crosslinking sites, which synergistically reinforced the existing chemical crosslinking network and caused the gel modulus to increase by nearly three orders of magnitude. This collaborative design, in which the chemical network provided the skeleton and the side-chain association acted as a switch, represented the core advantage of the pendant side-chain molecular strategy in this work. The chemical crosslinking network provided the basic mechanical skeleton, while the cardanol side chains independently responded to temperature changes as thermosensitive switches, and the two functions did not interfere with each other. The reversibility of this transition was verified through three consecutive heating–cooling cycles (25 ↔ 60 °C, Figure S2). This reversible behavior is structurally enabled by the fact that the covalent crosslinking locks in the spatial distribution of junction points while preserving the conformational freedom of the pendant C15 chains. Therefore, the C15 chains can reversibly associate and dissociate with temperature changes, while the covalent network topology remains fixed. The transition

width ($\Delta T_{10–90}$) is 8.5 °C with a hysteresis of 2.3 °C, and the response time is approximately 4 min. Compared to conventional systems such as methylcellulose (hysteresis ~22 °C) and Pluronic F127 (relaxation time ~10^4 s), this system exhibits significantly smaller thermal hysteresis and faster response, owing to the freely pendant cardanol side chains that enable rapid and concerted dehydration and hydrophobic association without large-scale structural reorganization [28,29]. A quantitative comparison with representative thermoresponsive materials is provided in Table S1 [30–33].

FT-IR analysis and sol fraction extraction were performed before and after heating at 60 °C for 24 h to distinguish the chemical and physical contributions. As shown in Figure 6a, the FT-IR spectra before and after heating overlapped almost completely, with no new characteristic absorption peaks appearing in regions such as C–N stretching (1100–1200 cm^{-1}) or N–H/O–H stretching (3000–3600 cm^{-1}), indicating that no new covalent bonds were formed during heating. The weak residual epoxide signal (3.8%) was not resolved in the hydrated gel spectra due to the overlap of broad water bands. The sol fraction remained statistically unchanged (9.9 ± 0.6% vs. 10.1 ± 0.5%, $p = 0.54$, not significant), which further supported this conclusion. As a result, it could be concluded that, for the prepared gel, the temperature-induced rheological enhancement was attributable to the reversible physical hydrophobic association of cardanol side chains rather than additional covalent network formation.

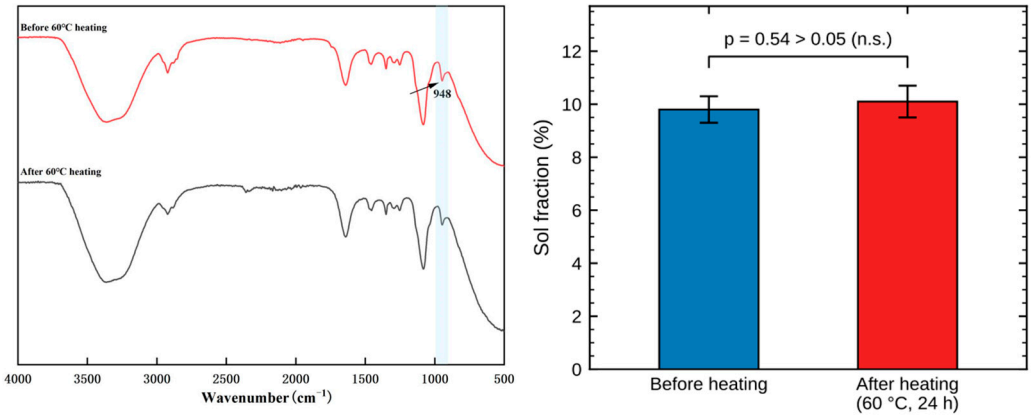


Figure 6. Deconvolution of chemical crosslinking and physical association.

After confirming that no new covalent bonds were formed during the heating of the prepared gel, the isothermal gelation process during preparation was further investigated. Although the gelation rate could be obtained from the rheological curves, the nucleation and growth of the gel network at the microscopic scale could not be revealed. Therefore, the Avrami kinetic model, which is used to describe phase transition processes, was introduced to analyze the gel formation process. The gelation process exhibited obvious temperature dependence and stage characteristics, as shown in Figure 7. When the temperature was below 25 °C, the G′ and G″ values of the system were very small and changed smoothly, and no obvious gelation reaction occurred. Once the temperature rose above the critical thermosensitive temperature of 35 °C, the gelation process began and developed through four stages, including the induction period, primary growth, secondary growth, and equilibrium period [34]. In the primary growth stage, G′ increased rapidly, indicating that the gel network had begun to form. In the secondary growth stage, the growth rate of G′ decreased, but G′ continued to increase, indicating that the gel network became more compact. After entering the equilibrium stage, G′ and G″ tended to be stable, indicating that the gel network structure had formed a complete and stable system. In addition, at 45 °C, G′ increased rapidly and the gelation time was short, indicating that the gelation

process was closely related to the temperature-dependent hydration state of PEG segments. Increasing temperature weakened PEG hydration and promoted hydrophobic association, thereby accelerating network formation and stabilization.

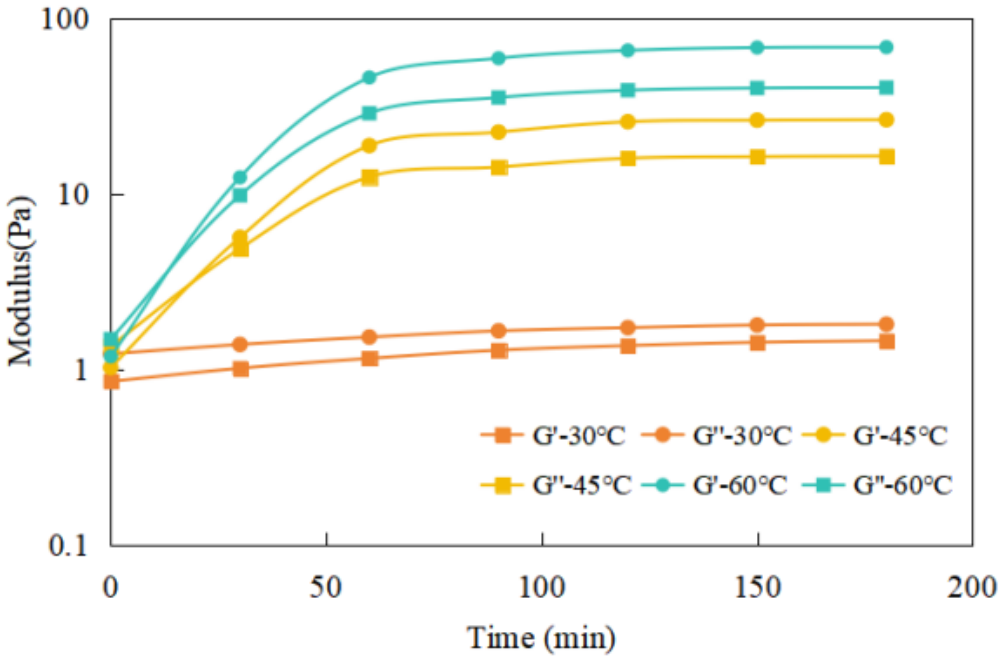


Figure 7. Rheological properties of the gelation process of the thermosensitive polyamine gel system.

The possible simultaneous occurrence of chemical crosslinking and physical hydrophobic association during preparation was further examined by Avrami kinetic fitting, which was performed over the range of 30–60 °C, and the gelation growth factors at different temperatures were obtained, as shown in Figure 8a–c. The exponents for the primary stage (n_1) ranged from 0.85 to 0.98, and those for the secondary stage (n_2) ranged from 1.08 to 1.28. These low values ($n < 1.5$) are below the classical Avrami exponents for homogeneous crystallization. We interpret n_1 and n_2 as empirical descriptors of the two-stage densification kinetics rather than geometric dimensionality indicators. The poor linearity of the Arrhenius fits ($R^2 = 0.62$ and 0.35) suggests that the gelation process is not governed by a simple thermally activated phase transition, but rather by the synergistic interplay between chemical crosslinking and temperature-sensitive physical hydrophobic association.

Arrhenius fitting was performed on the growth rate constants of the thermosensitive gel system at different temperatures, as shown in Figure 8d. It was observed that a physically meaningful apparent activation energy cannot be reliably extracted from these fits. This result is consistent with the proposed dual-mechanism involving temperature-induced dehydration of PEG segments and hydrophobic association of the pendant C15 chains. The poor Arrhenius linearity is consistent with an additional kinetic barrier associated with dehydration of the side chains, rather than a single thermally activated process. However, this barrier is not quantified from the present Arrhenius fits. This further confirmed, from a kinetic perspective, the role of cardanol side chains as independent thermosensitive units. The sensitivity of the fitted parameters to the t0 criterion is provided in Figure S3.

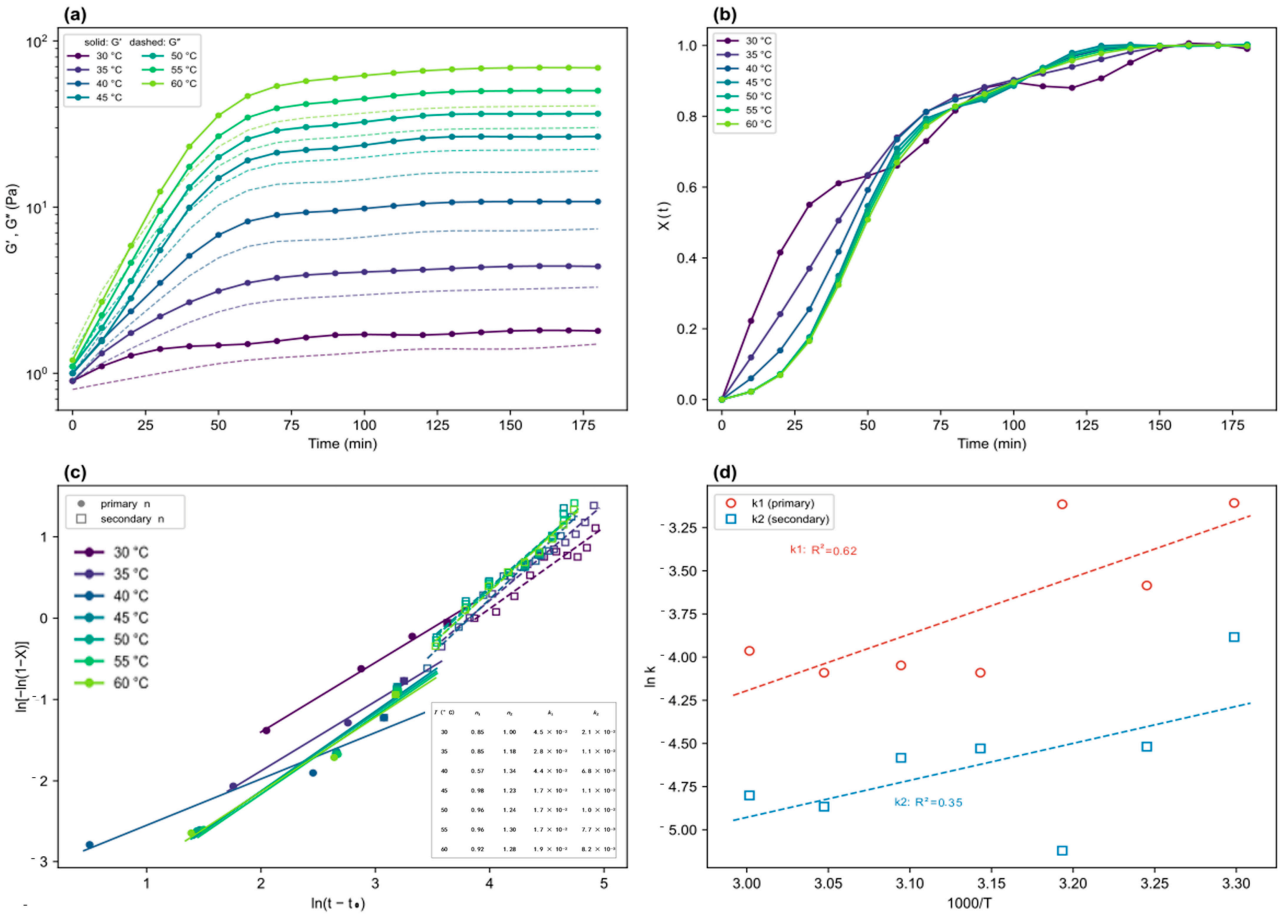


Figure 8. Kinetic analysis of the thermosensitive gel system. (**a**) G′(t) and G′′(t) curves; (**b**) X(t) transformation plots; (**c**) Avrami plots; (**d**) Arrhenius plot of the growth rate constants.

The effect of salinity on the thermosensitive gelation process was mainly kinetic regulation rather than thermodynamic change. Figure 9 shows that the effect of salinity on the gelation process occurred throughout the induction, gelation, and maturation stages, and the response patterns differed among these stages. In the induction stage, the induction period exhibited a non-monotonic variation, first decreasing and then increasing with increasing salinity. When salinity increased from 0 to 3000 mg/L, the induction period was shortened by approximately 40%, corresponding to a reduction of 12.5 min. This was attributed to the synergistic promotion by weak electrostatic screening and slight salting-out under low-salinity conditions. Na^+ and Cl^- moderately screened the positive charges of amino groups, reducing interchain electrostatic repulsion. Meanwhile, the salting-out effect thinned the hydration layer around the long hydrophobic alkyl chains of cardanol, allowing the hydrophobic segments to form initial physical crosslinking nuclei in a more ordered manner, thereby reducing the nucleation energy barrier for chemical crosslinking. However, when salinity further increased to 5000 mg/L, the induction period was prolonged by an increase of 10 min. This resulted from strong charge screening, which caused severe chain coiling and buried the active sites of epoxy and amino groups. In addition, excessive salting-out dehydration of PEG segments reduced diffusion efficiency. The cardanol hydrophobic chains locally over-aggregated into nonuniform hydrophobic clusters, disrupting network continuity. By controlling salinity, the migration time of the gel solution could be regulated within a certain range, with low salinity shortening the induction period and relatively high salinity prolonging it.

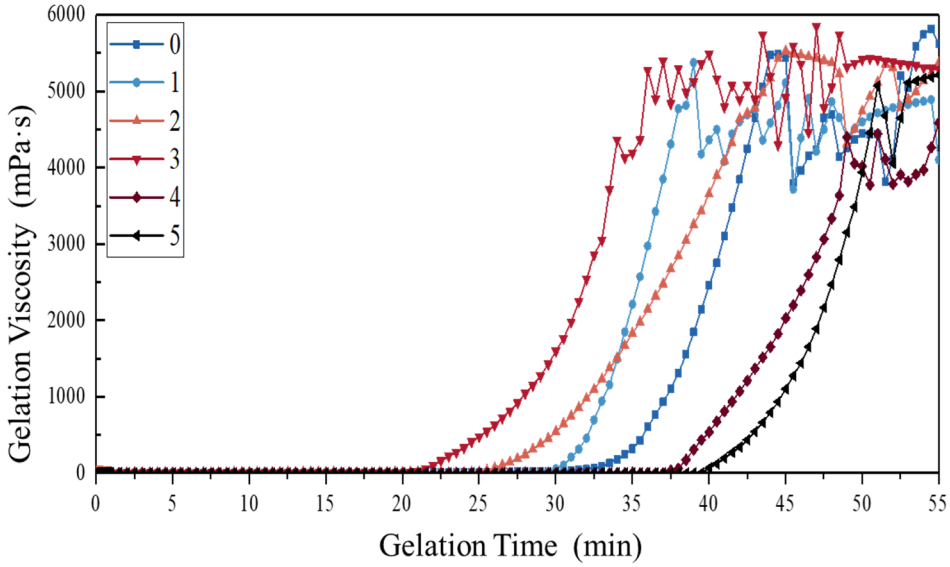


Figure 9. Regulation of gelation kinetics of cardanol-based thermosensitive hydrogel by salinity.

The gelation period increased monotonically with increasing salinity, which was attributed to the strong hydration characteristics of the PEG main chain and the diffusion-controlled nature of the crosslinking reaction [35,36]. PEG segments formed strong hydrogen-bonding networks with water molecules through ether oxygen atoms, constructing a thick hydration layer around them and maintaining chain extension and molecular diffusion. As strongly hydrating ions, salt ions stripped bound water from the PEG surface and compressed the hydration layer through solvent competition and salting-out effects. This weakened PEG hydration, changed the chain conformation from extended to coiled, reduced the hydrodynamic radius, and slowed molecular diffusion. Since the crosslinking reaction between epoxy and amino groups is essentially diffusion-controlled, a decrease in diffusion rate directly reduced the effective collision frequency, thus prolonging the gelation period with increasing salinity.

During the maturation stage, the measured G′ plateau values were similar across the investigated NaCl concentrations of 0–5000 mg/L at 45 °C. This observation suggests that, within these experimental conditions, NaCl concentration affected gelation kinetics more prominently than the final plateau modulus. The conclusion is restricted to the tested electrolyte composition, concentration range, and observation period.

Actual formation waters contain mixtures of ionic species whose effects cannot be represented by total salinity alone. Ca^{2+} and Mg^{2+} may influence PEG hydration, ionic screening, and hydrophobic association through ion-specific interactions. These are potential contributions requiring verification in the present gel system. The simulated formation brine used for the plugging experiment contained approximately 18.2 mg/L Mg^{2+} and 40.1 mg/L Ca^{2+}, calculated from the salt dosages in Table 1. The plugging results therefore demonstrate performance under this selected mixed-brine condition. However, the specific evolution of the induction time and final storage modulus under higher divalent-ion concentrations cannot be quantitatively predicted from the present dataset, as the reported findings are strictly confined to the tested electrolyte composition and concentration range. The origin of this counterintuitive phenomenon lies in three aspects. First, the total amounts of epoxy and amino functional groups in the system were fixed by the formulation stoichiometry, and the PEG main chain had excellent chain flexibility. Even if some active sites were temporarily buried under elevated salinity, they could be gradually unlocked and participate in crosslinking as the reaction proceeded. Therefore, the final conversion of chemical crosslinking and the total crosslinking density were basically similar under different salini-

ties. Second, salt exerted a bidirectional competition on physical crosslinking. Under low salinity, hydrophobic association was enhanced but hydrogen bonding was weakened. With the increase in salinity, hydrophobic aggregation was enhanced but hydrogen bonding was competitively disrupted. These two effects offset each other, and the net contribution of physical crosslinking remained relatively stable. Third, salt only changed the microscopic network morphology and hydrophobic microdomain distribution of the gel, whereas conventional steady-state viscosity measurements provided a macroscopic average response and were insensitive to microscopic structural differences. The above results indicated that within the tested NaCl concentration range, the thermosensitive phase transition driven by the thermally induced hydrophobic association of cardanol side chains remained effective, and the final equilibrium network strength was not significantly altered after complete maturation. Salinity primarily changed the gelation kinetic pathway under the investigated conditions. Within the tested NaCl concentration range (0–5000 mg/L), salinity primarily modulated the gelation kinetics rather than the thermosensitive phase transition capability, while the measured equilibrium plugging performance remained comparatively stable under the investigated conditions.

Table 1. Composition of simulated formation brine.

Formula	NaCl	$NaHCO_3$	KCl	$MgCl_2 \cdot 6H_2O$	$CaCl_2$	Na_2CO_3	Na_2SO_4
Dosage (mg/L)	2898	1400	219.5	152.5	111	183	50

2.3. Temperature-Triggered Plugging Performance in Porous Media

The thermally induced hydrophobic association of cardanol side chains could achieve temperature-controlled reinforcement based on the chemically crosslinked network, as demonstrated by the above thermosensitive phase transition behavior and rheological analysis. The temperature-responsive characteristic was the core driving force for deep fluid diversion in this gel system. A baseline test of the temperature-dependent intrinsic plugging capability was first conducted in an ultrapure water system to exclude salinity interference and to verify the practical engineering adaptability under target reservoir conditions (60 °C, 5014 mg/L). As shown in Figure 10, at low temperatures between 25 and 35 °C, the precursor solution exhibited excellent injectivity, and the plugging rate remained at a low level (<20%). This phenomenon was attributed to the dense hydration layer surrounding the long alkyl chains of cardanol at low temperatures. The chains existed in a dispersed state around the polymer backbone and could not form an effective intermolecular hydrophobic association. The developed side-chain gel system remained in a low-viscosity sol state and exhibited minimal flow resistance when migrating through porous media.

When the temperature increased to 40 °C, the system crossed the critical phase transition temperature, and the plugging rate sharply increased to 72.3%. The sharp increase in the plugging rate resulted not from a simple thermodynamic expansion effect but from a network structural transition triggered by temperature-induced dehydration. The ordered hydration shell around the C15 long alkyl chains was disrupted, hydrophobic driving forces became dominant, and the side chains spontaneously aggregated to form numerous dynamic physical crosslinking microdomains [37]. These physical nodes interpenetrated with the DETA/PEGO covalent crosslinking skeleton, endowing the gel with highly elastic response characteristics. The increase in plugging efficiency accompanies the thermally induced rheological strengthening of the gel system. However, the flooding results do not directly distinguish the contributions of adsorption, hydrodynamic retention, and pore-space obstruction.

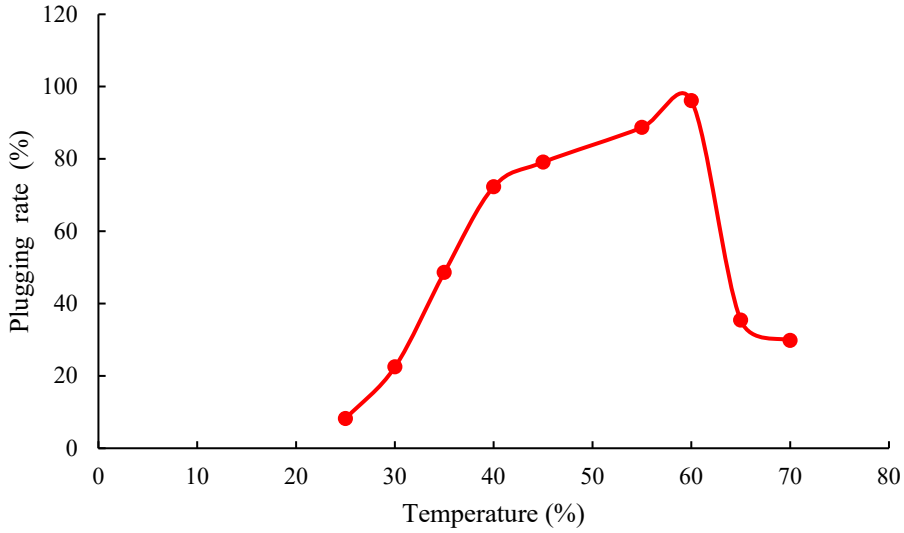


Figure 10. Effect of temperature on plugging rate of cardanol-based gel system.

From 45 to 60 °C, the plugging rate increased continuously and reached a peak of 96.1% at 60 °C. This temperature range matched the target reservoir temperature, indicating that the thermally induced hydrophobic association window of the cardanol side chains was well matched to the target reservoir temperature range and confirming the reservoir adaptability of the molecular design. In this temperature range, the thermal motion energy barrier of cardanol side chains and the hydrophobic stacking rate reached an optimal match. The formed hydrophobic clusters had a uniform size and dense spatial distribution, the synergistic efficiency of chemical crosslinking and physical association was maximized, and the most complete dual-network reinforcement structure was constructed. However, when the temperature further increased to 65 °C, the plugging rate dropped to 35.4%. The decrease in plugging efficiency at 65 °C indicates reduced performance at elevated temperatures under the tested conditions. Changes in PEG hydration and hydrophobic aggregation may contribute to this behavior; however, network collapse was not directly demonstrated. Such changes could promote network compaction or heterogeneous reorganization, potentially reducing effective pore occupancy or contact with the surrounding grains and allowing preferential water-flow pathways to develop. This provides a possible explanation for reduced plugging efficiency despite increased local hydrophobic association. The measurements at 60 and 65 °C do not establish the exact onset temperature of performance deterioration. The significant decrease at 65 °C, which is only 5 °C above the target reservoir temperature, suggests a relatively narrow operational safety margin. For field application, the expected local temperature range and gradients should therefore be carefully considered. Since the temperature series in Figure 10 was obtained using deionized water, further validation under the relevant temperature and formation-water conditions is required.

Figure 11 demonstrates the engineering adaptability of the thermosensitive cardanol gel under simulated target reservoir conditions. At the initial injection stage (10 min), the damage rate of the core was only 10.02%, and the permeability decreased from 574 to 516.5 mD. This extremely low flow resistance directly confirmed the kinetic conclusion of the prolonged induction period under salinity observed in the previous salinity-dependent gelation analysis. Under a salinity of 5014 mg/L, strong charge screening caused severe chain coiling, severely damaged the PEG hydration layer, and buried the active epoxy and amino sites. The induction period was extended by approximately 30% compared with the low-salinity system. The limited permeability reduction during the first 10 min indicates that substantial plugging had not yet developed under the tested laboratory conditions. This observation does not establish the influence of field shear conditions on gelation or

demonstrate avoidance of premature near-wellbore plugging. As the time after injection increased to 20–40 min, the system crossed the induction period and entered the gelation period, and the gel network began to form and densify rapidly. The damage rate increased to 47.07% at 20 min with the permeability decreasing to 303.8 mD, to 81.36% at 30 min with the permeability decreasing to 107 mD, and further to 99.22% at 40 min. During this stage, the strong salting-out effect under salinity promoted significant hydrophobic association of the long alkyl chains of cardanol. Chemical crosslinking and physical hydrophobic crosslinking were synergistically enhanced. The macromolecular network was effectively retained in the core pore throats and greatly reduced the water-phase permeability.

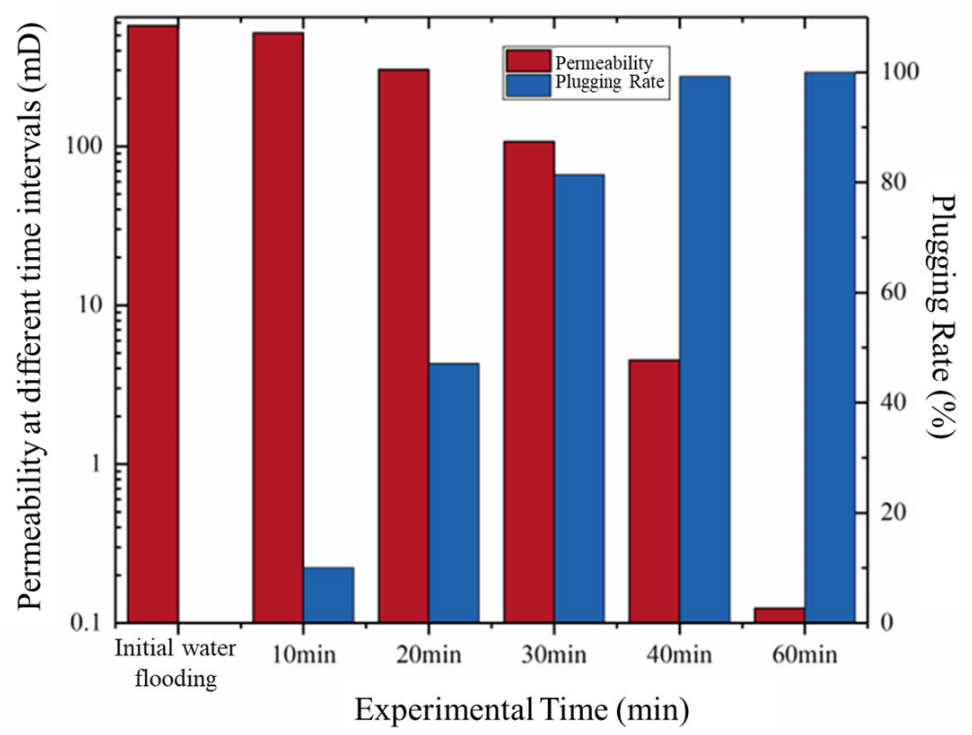


Figure 11. Plugging performance evaluation of the gel system at 60 °C and salinity of 5014 mg/L.

When the time after injection reached 60 min, the system fully entered the maturation period. The damage rate reached 99.98%, and the permeability decreased to 0.124 mD, forming nearly absolute plugging. The slight difference between the two values mainly originated from the difference in test conditions. Figure 10 describes the equilibrium plugging rate measured in an ultrapure water system after aging, while Figure 11 shows in situ solidification of the gel in the porous media inside the core under salinity conditions. The substantial permeability reduction demonstrates effective plugging under the investigated conditions. Nevertheless, the present measurements do not establish the dominant pore-scale retention mechanism or directly demonstrate accelerated network densification within the porous medium. The effect of salinity on the gel system was mainly reflected at the kinetic level. Although salinity significantly prolonged the early injection window, that is, the induction period, it did not significantly alter the equilibrium network strength after complete maturation, indicating a tunable kinetic process with a comparatively stable equilibrium result under the investigated conditions. The rapid and controllable plugging establishment exhibited by the gel under simulated reservoir-brine conditions lays a foundation for its application in deep fluid diversion in moderate-temperature reservoirs with saline formation water. The plugging results establish performance within the investigated aging periods.

Furthermore, the gel exhibited stable performance after 30 days of aging at 60 °C, with a modulus retention of 94.0% and a plugging rate of 98.2% (Figure S4). During prolonged aging, changes in network hydration and hydrophobic-domain organization could promote contraction and water expulsion, potentially impairing plugging performance. Stability beyond 30 days has not been determined and requires extended aging tests. In addition, the porous-media evaluation was conducted using a single core with a permeability of 574 mD. The applicability of the gel to cores with different permeabilities, as well as its performance under repeated flooding cycles and post-treatment pressure resistance, requires systematic investigation in future work.

Although the temperature-dependent plugging performance has been demonstrated, the specific contribution of the cardanol C15 chains requires further clarification. A control hydrogel without cardanol was prepared and tested to further verify the origin of the thermoresponsive plugging behavior. As shown in Figure 12, the control gel still forms a stable covalent network but exhibits no temperature responsiveness in transmittance, G′, swelling ratio, or plugging rate. In contrast, the cardanol-modified gel shows a clear thermoresponsive transition across all four measurements. This direct comparison confirms that the phase transition and the subsequent plugging performance originate exclusively from the hydrophobic association of the freely pendant C15 chains, rather than the PEG backbone. Furthermore, the conventional chromatographic separation of crosslinkers is not applicable to this system because both the prepolymer and PEGO are small molecules of comparable size, the difference in their size-exclusion partition coefficients within the porous media is negligible, allowing them to co-transport as a single slug [38]. In addition, the behavior of the gel in the presence of crude oil was evaluated, demonstrating effective wettability reversal and deep plugging capability in oil-wet porous media (Figure S5).

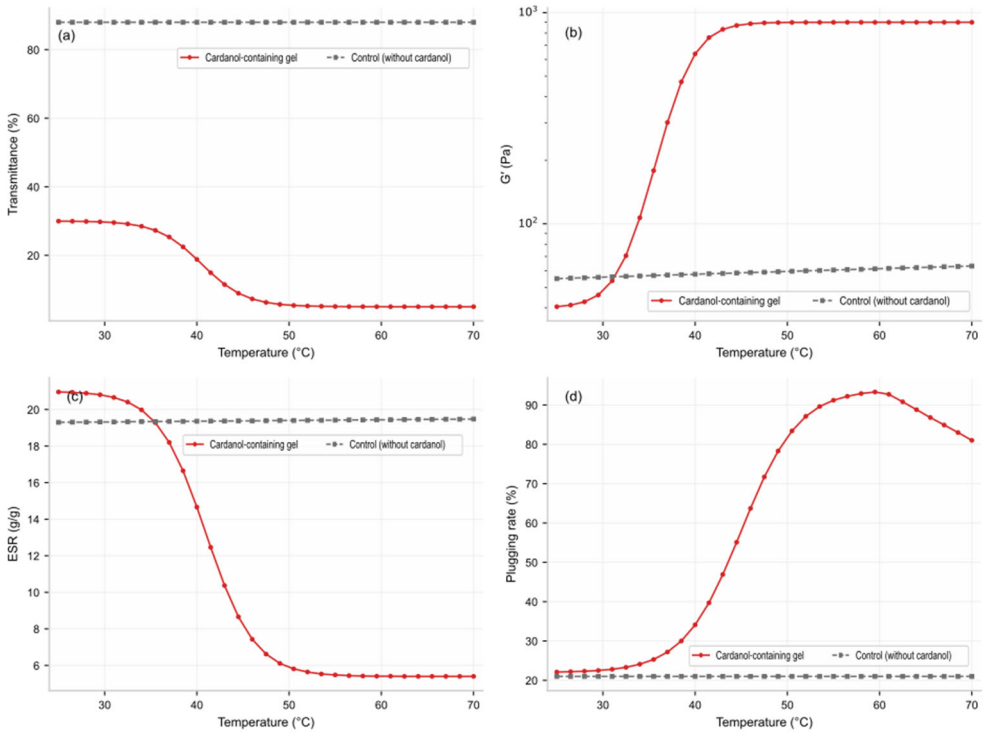


Figure 12. Thermoresponsive comparison between the cardanol-modified gel and the control gel without cardanol: (**a**) transmittance, (**b**) storage modulus G′, (**c**) equilibrium swelling ratio (ESR), and (**d**) plugging rate as a function of temperature.

3. Conclusions

This study developed a cardanol side-chain hydrophobic association thermosensitive hydrogel to address the trade-off between gelation controllability and equilibrium performance in moderate-temperature saline reservoirs. Unlike existing systems where alkyl chains are embedded in the backbone or fixed at crosslinking nodes, cardanol units were grafted as freely pendant side groups onto a chemically crosslinked polyamine backbone, allowing C15 chains to escape topological constraints and act as independent thermoresponsive switches, while the PEGO/DETA network provides a stable mechanical skeleton. Thermal activation drives pronounced network evolution: the storage modulus increases by nearly three orders of magnitude to approximately 980 Pa, and transmittance drops from 28.9% to below 4%. Kinetic analysis indicates a transition from diffusion-controlled to chemically controlled network growth, with the Avrami exponent n ranging from 0.85 to 1.28 across the tested temperatures. The non-Arrhenius behavior ($R^2 = 0.62$ and 0.35) reflects the synergistic dual mechanism of chemical crosslinking and physical association. The deviation from classical Arrhenius behavior is consistent with the additional kinetic barrier associated with the dehydration of the hydrophobic side chains. Within the investigated NaCl concentration range of 0–5000 mg/L at 45 °C, salt concentration affected gelation kinetics more prominently than the measured plateau storage modulus. This finding is specific to the tested conditions, and its applicability to formation waters with different ionic compositions, particularly different Ca^{2+} and Mg^{2+} concentrations, requires further evaluation. Sand-pack flooding tests showed a plugging rate of 96.1% at 60 °C in deionized water, and in situ gelation in the core under simulated target-reservoir formation water at 60 °C and 5014 mg/L reduced permeability by 99.98% within 60 min. This cardanol-derived dual-network hydrogel offers an efficient solution for deep fluid diversion in moderate-temperature saline reservoirs and establishes a design principle of chemical network as skeleton and side-chain association as switch, providing new insights for next-generation intelligent oilfield chemicals incorporating cardanol-derived components.

4. Materials and Methods

4.1. Materials

The following materials and reagents were used in this study to conduct the experiments. Diethylenetriamine of analytical grade with a purity ≥ 99.0% was purchased from Shanghai Aladdin Biochemical Technology Co., Ltd. (Shanghai, China). Cardanol of industrial grade was derived from cashew nut shell liquid with m-pentadecylphenol as the main component and was purchased from Hubei Xingyan Materials Technology Co., Ltd. (Wuhan, China). Epichlorohydrin of analytical grade with purity ≥99.5%, sodium hydroxide (≥96.0%), anhydrous ethanol (≥99.7%), hydrochloric acid (36.0–38.0%) and other reagents (all of analytical grade) were purchased from Sinopharm Chemical Reagent Co., Ltd. (Shanghai, China). Tetrabutylammonium bromide (analytical grade, purity ≥99.0%) and polyethylene glycol diglycidyl ether (purity ≥95%, epoxy value 0.35–0.40 eq/100 g, Mn ≈ 600) were purchased from Shanghai Macklin Biochemical Co., Ltd. (Shanghai, China). The water used for hydrogel preparation was ultrapure water. Simulated formation brine was used only for preparing the gel in the salinity-tolerance flooding tests, and its composition was given in Table 1.

4.2. Experimental Methods

4.2.1. Synthesis of Cardanol Glycidyl Ether

Cardanol glycidyl ether was synthesized through a one-step method. A total of 0.1 mol cardanol, 0.12 mol epichlorohydrin, and 0.005 mol tetrabutylammonium bromide were

added to a 250 mL three-necked round-bottom flask equipped with a stirrer, a thermometer, and a reflux condenser. Tetrabutylammonium bromide served as a phase-transfer catalyst. The mixture was stirred vigorously at 60 °C until a homogeneous system formed. Subsequently, a 30 wt% aqueous sodium hydroxide solution prepared from 0.11 mol sodium hydroxide was slowly added dropwise into the reaction system over 2 h using a constant-pressure dropping funnel. The reaction temperature was maintained below 65 °C. After the addition was complete, the reaction was continued at 60 °C for 6 h.

After the reaction, the mixture was cooled to room temperature and neutralized with an appropriate amount of dilute hydrochloric acid until neutral. Then, the mixture was washed three times with deionized water to remove salts. The organic phase was collected, and excess epichlorohydrin and water were removed under reduced pressure using a rotary evaporator at 70 °C to give a reddish-brown viscous liquid, which was cardanol glycidyl ether.

4.2.2. Preparation and Structural Characterization of Cardanol-Modified Thermosensitive Hydrogel

The target hydrogel was prepared by a prepolymer-crosslinking method, as shown in Figure 13, and all procedures were carried out in a fume hood. First, the prepolymer was prepared. A 100 mL three-necked flask was charged with 0.02 mol (2.06 g) diethylenetriamine and 20 mL anhydrous ethanol, and the mixture was stirred on a magnetic stirrer until dissolved. The flask was placed in an ice-water bath and cooled to 0–5 °C. Then, 0.01 mol (4.2 g) cardanol glycidyl ether was weighed, diluted with 10 mL anhydrous ethanol, and transferred to a constant-pressure dropping funnel. Under continuous vigorous stirring, the ethanol solution of cardanol glycidyl ether was slowly added dropwise to the diethylenetriamine solution at approximately 1–2 drops per second, and the reaction temperature was strictly maintained below 10 °C. The dropwise addition took approximately 1.5 h. After the addition was complete, the ice-water bath was removed, and the reaction mixture was allowed to warm naturally to room temperature and was continuously stirred for 2 h. Subsequently, the reaction system was transferred to a 45 °C oil bath and reacted for an additional 6 h. After the reaction, the mixture was distilled under reduced pressure using a rotary evaporator at 50 °C and −0.1 MPa to remove ethanol and excess diethylenetriamine, affording an amber viscous cardanol-diethylenetriamine prepolymer, which was sealed and stored for further use.

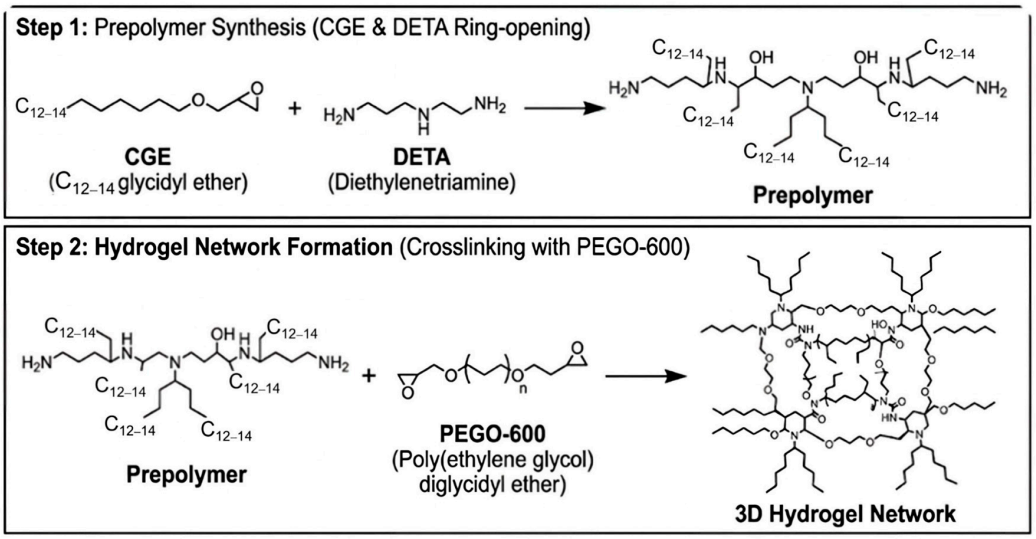


Figure 13. Schematic diagram of the synthesis of cardanol-modified thermosensitive hydrogel.

Then, the hydrogel was prepared. The synthesized prepolymer and a stoichiometric amount of polyethylene glycol diglycidyl ether were separately dissolved in ultrapure water or simulated formation water to prepare 20 wt% solutions. The two solutions were mixed at a molar ratio of amine groups to epoxy groups of 1 to 1 and stirred rapidly for 2 min. The mixed solution was poured into a specific mold and kept statically in an oven at 45 °C for 48 h to obtain the final cardanol-modified thermosensitive hydrogel. This curing temperature was chosen to balance the epoxy–amine reaction kinetics (ensuring complete curing within 48 h with a practical induction period) and the intentional pre-organization of the pendant C15 chains, which begin to aggregate just above their association temperature. Subsequently, the chemical structure and micromorphology of the prepared cardanol-modified thermosensitive hydrogel were characterized. Nuclear magnetic resonance spectra were recorded on a JNM-ECZ500R NMR spectrometer (JEOL, Tokyo, Japan). The prepolymer sample was dissolved in deuterated chloroform and analyzed by ^{1}H NMR and ^{13}C NMR to confirm its chemical structure. Fourier transform infrared spectra were recorded on a Nicolet iS50 FT-IR spectrometer (Thermo Fisher Scientific, Madison, WI, USA) in attenuated total reflectance mode over a scan range of 4000–500 cm^{-1} with a resolution of 4 cm^{-1}, and dried gel samples were analyzed for functional groups. Scanning electron microscopy was used to characterize the micromorphology of hydrogel samples. Furthermore, the sol fraction of the gel before and after heating at 60 °C for 24 h was determined by a solvent extraction method. The chemical structure before and after heating was characterized by FT-IR. The epoxy conversion at 45 °C was evaluated based on the variation in the characteristic FT-IR epoxide peak.

4.2.3. Thermosensitive Phase Transition Behavior and Gelation Kinetics Characterization

Transmittance and rheological measurements were conducted to characterize the thermosensitive phase transition behavior of the gel and the accompanying rheological response. Transmittance measurements were performed using a UV-2600 ultraviolet-visible spectrophotometer (Shimadzu, Kyoto, Japan). The gel solution was placed in a quartz cuvette equipped with a thermostatted water jacket, and the transmittance was recorded as a function of temperature from 25 to 70 °C at a heating rate of 0.5 °C/min at a wavelength of 560 nm.

Rheological measurements were performed using a DHR-2 rotational rheometer (TA Instruments, New Castle, DE, USA) with parallel-plate geometry, a diameter of 40 mm, and a gap of 1 mm. First, a stress sweep was conducted to determine the linear viscoelastic region. Then, a temperature sweep was conducted from 20 to 70 °C at a heating rate of 1 °C/min at a fixed angular frequency of 6.28 rad/s and a strain of 1%, and the storage modulus (G') and loss modulus (G'') were recorded.

The Avrami kinetic model was applied to fit the rheological data of the gelation process, using the change rate of the complex modulus to represent the gel volume fraction. The Avrami exponent n and gelation rate constant k were obtained by fitting.

$$X(t) = 1 - \exp(-kt^n) \quad (1)$$

$$X(t) = \frac{G*(t) - G*(0)}{G*(\infty) - G*(0)} \quad (2)$$

$$\ln(-\ln[1 - X(t)]) = \ln k + n\ln(t - t_0) \quad (3)$$

where $G^*(0)$ was the initial complex modulus; $G^*(\infty)$ was the equilibrium complex modulus and t_0 was the induction time for gel nucleation.

Kinetic parameters n and k were obtained by linear fitting of the experimental data under different conditions, thereby allowing the growth mode and reaction rate of the gel to be quantitatively elucidated. An Arrhenius plot of ln k versus $1/T$ was constructed using the k values determined at different temperatures, and the apparent activation energy E_a of the gelation process was calculated from the slope.

$$\ln k = \ln A - \frac{E_a}{RT} \quad (4)$$

where A was the frequency factor; R was the molar gas constant; and T was the thermodynamic temperature.

The effect of salinity on gelation kinetics was investigated by adding NaCl in increments of 1000 mg/L during gel preparation to adjust the system salinity from 0 to 5000 mg/L. The same rheological test method described above was used to monitor the changes in G′ and G″ over time at a constant temperature of 45 °C. For comparison, a control hydrogel without cardanol was prepared using the identical procedure, except that CGE was omitted. The PEGO and DETA were mixed and reacted under the same conditions, and the resulting control gel was subjected to the same transmittance, rheological, and swelling measurements as described in this section. To quantitatively describe the effect of salinity on each gelation stage, the gelation process was divided into an induction period, a gelation period, and a maturation period. The induction period is defined as the time from the start of mixing to the onset of a significant increase in G′. The gelation period is defined as the time from the end of the induction period to the gel point, at which G′ surpasses G″. The induction period is defined as the time from the start of mixing to the onset of a significant increase in G′. The gelation period spans from the end of the induction period to the gel point, at which G′ surpasses G″. The maturation period corresponds to the equilibrium stage after G′ reaches its plateau value.

4.2.4. Single-Tube Sand-Pack Plugging Experiments

The plugging performance of the gel was evaluated using a single-tube sand-pack model at a water flooding rate of 0.3 mL/min. The model dimensions were 2.5 cm in diameter and 10.1 cm in length, and the initial water permeability was 574 mD.

The effect of temperature on the plugging performance was investigated over the range of 25–65 °C. The gel solution was prepared with distilled water to eliminate salinity interference and isolate the effect of temperature. A volume of 1 PV of the gel solution was injected at 0.3 mL/min, and the model was then aged at the set temperature for 24 h. After aging, subsequent water flooding was performed at the same flow rate. The water permeability before and after aging was recorded, and the plugging rate R was calculated using the following equation.

$$R = \frac{k_1 - k_2}{k_1} \times 100\% \quad (5)$$

The salt tolerance of the gel was further examined. The gel solution was prepared using simulated formation water at 60 °C. After 1 PV of the gel solution was injected at 0.3 mL/min, the model was aged at 60 °C, and the model permeability was measured at different time points within 60 min after injection to calculate the plugging rate. This experiment verified whether the thermosensitive plugging performance of the gel remained effective under simulated reservoir salinity conditions. The control hydrogel was subjected to the same sand-pack plugging evaluation under identical conditions.

Supplementary Materials: The following supporting information can be downloaded at https://www.mdpi.com/article/10.3390/gels12110982/s1, Figure S1. Quantitative pore-size statistics of the freeze-dried gel; Figure S2. (a) G′ over three heating–cooling cycles (25 ↔ 60 °C); (b) plateau G′ at 60 °C per cycle (<1 % drift); Figure S3. Sensitivity of the fitted parameters to the t_0 criterion. (a) n_1 vs. t_0 threshold; (b) k_1 vs. t_0 threshold; Figure S4. Long-term thermal stability of the gel over 30 days at 60 °C in 5014 mg/L simulated formation brine. (a) G′ retention, (b) syneresis, and (c) plugging rate after aging; Figure S5. Evaluation of the gel behavior in the presence of crude oil. (a) Water contact angles on oil-wet surfaces before and after precursor treatment. (b) Temperature-dependent storage modulus (G′) with 0–30 vol% crude oil. (c) Plugging rates in water-wet and oil-wet sand packs at 60 °C; Table S1. Comparison of thermoresponsive characteristics of the cardanol-modified gel with representative literature systems.

Author Contributions: Conceptualization, J.M., X.L. (Xiangbin Liu). and B.Z. (Baize Zhu); methodology, J.M., G.M. and Q.L.; investigation, Q.L.; data curation, J.M. and Z.Z.; writing—original draft, J.M. and X.L.(Xuesong Lin); writing—review and editing, Z.Z., G.M. and L.W.; supervision, Q.L., Z.Z., G.M. and B.Z.(Baize Zhu); formal analysis, Q.W., B.Z.(Biao Zhang) and Q.Z. All authors have read and agreed to the published version of the manuscript.

Funding: This research received no external funding.

Institutional Review Board Statement: Not applicable.

Informed Consent Statement: Not applicable.

Data Availability Statement: The original contributions presented in the study are included in the article and Supplementary Materials. Further inquiries can be directed to the corresponding author.

Acknowledgments: This research was conducted at the Research Institute of Oil Production Engineering, Daqing Oilfield Limited Company (Daqing, China).

Conflicts of Interest: Authors Jianxun Meng, Xiangbin Liu, Qingsong Li, Zhixuan Zhu, Qingguo Wang, Qi Zhou, Baize Zhu, Biao Zhang, Xuesong Lin, and Lichao Wang were employed by Daqing Oilfield Limited Company. Author Guoliang Mao declares that the research was conducted in the absence of any commercial or financial relationships that could be construed as a potential conflict of interest.

References

1. Song, Z.; Hou, J.; Zhang, L.; Chen, Z.; Li, M. Experimental study on disproportionate permeability reduction caused by non-recovered fracturing fluids in tight oil reservoirs. *Fuel* **2018**, *226*, 627–634. [CrossRef]
2. Jiang, T.; Shen, Z.; Wang, L.; Qi, Z.; Xiao, B.; Qin, Q.; Fan, X.; Wang, Y.; Qu, H. Optimization method of fracturing fluid volume intensity for SRV fracturing technique in shale oil reservoir based on forced imbibition: A case study of well X-1 in Biyang Sag of Nanxiang Basin, China. *Pet. Explor. Dev.* **2024**, *51*, 674–683. [CrossRef]
3. Lu, S.; Bo, Q.; Zhao, G.; Shaikh, A.; Dai, C. Recent advances in enhanced polymer gels for profile control and water shutoff: A review. *Front. Chem.* **2023**, *11*, 1067094. [CrossRef] [PubMed]
4. Xu, Z.; Zhao, M.; Xie, Y.; Li, T.; Meng, X.; Dong, Y.; Yang, Z.; Dai, C. Nanoslickwater fracturing fluid with enhanced imbibition capacity for low-permeability reservoirs. *Energy Fuels* **2025**, *39*, 1141–1151. [CrossRef]
5. Yang, J.; Wu, T.; Liu, Q.; Huang, H.; Chen, S.; Chen, G. Research of a fracturing-oil displacement integrated working fluid based on betaine surfactant. *Colloids Surf. A Physicochem. Eng. Asp.* **2024**, *686*, 133371. [CrossRef]
6. Dai, C.; Wang, K.; Liu, Y.; Li, H.; Wei, Z.; Zhao, M. Reutilization of fracturing flowback fluids in surfactant flooding for enhanced oil recovery. *Energy Fuels* **2015**, *29*, 2304–2311. [CrossRef]
7. Sun, J.; Xu, C.; Kang, Y.; Jing, H.; Zhang, J.; Yang, B.; You, L.; Zhang, H.; Long, Y. Formation damage mechanism and control strategy of the compound function of drilling fluid and fracturing fluid in shale reservoirs. *Pet. Explor. Dev.* **2024**, *51*, 430–439. [CrossRef]
8. Al Brahim, A.; Bai, B.; Schuman, T. Comprehensive review of polymer and polymer gel treatments for natural gas-related conformance control. *Gels* **2022**, *8*, 353. [CrossRef] [PubMed]
9. Wang, F.; Xu, H.; Liu, Y.; Meng, X.; Liu, L. Non-linear seepage model of hydraulic fracturing assisted oil displacement coupled with effects of high-pressure reduced adsorption: A case study of low and medium permeability reservoirs in Daqing Oilfield, NE China. *Pet. Explor. Dev.* **2024**, *51*, 1564–1573. [CrossRef]
10. Tanaka, T. Collapse of gels and the critical endpoint. *Phys. Rev. Lett.* **1978**, *40*, 820–823. [CrossRef]

11. Qiao, S.-L.; Mamuti, M.; An, H.-W.; Wang, H. Thermoresponsive polymer assemblies: From molecular design to theranostics application. *Prog. Polym. Sci.* **2022**, *131*, 101578. [CrossRef]
12. Zhang, K.; Xue, K.; Loh, X.J. Thermo-responsive hydrogels: From recent progress to biomedical applications. *Gels* **2021**, *7*, 77. [CrossRef] [PubMed]
13. Lv, T.; Chen, Y.; Li, N.; Liao, X.; Heng, Y.; Guo, Y.; Hu, K. A comprehensive review of thermosensitive hydrogels: Mechanism, optimization strategies, and applications. *Gels* **2025**, *11*, 544. [CrossRef] [PubMed]
14. Kang, W.; Kang, X.; Lashari, Z.A.; Li, Z.; Zhou, B.; Yang, H.; Sarsenbekuly, B.; Aidarova, S. Progress of polymer gels for conformance control in oilfield. *Adv. Colloid Interface Sci.* **2021**, *289*, 102363. [CrossRef] [PubMed]
15. Zhu, D.; Bai, B.; Hou, J. Polymer gel systems for water management in high-temperature petroleum reservoirs: A chemical review. *Energy Fuels* **2017**, *31*, 13063–13087. [CrossRef]
16. Wang, K.; Luo, M.; Li, M.; Gu, X.; Li, X.; Fan, Q.; Pu, C.; Wang, L. Gelation and plugging performance of low-concentration partially hydrolyzed polyacrylamide/polyethyleneimine system at moderate temperature and in fractured low-permeability reservoir. *Polymers* **2024**, *16*, 1585. [CrossRef] [PubMed]
17. Liu, Y.; Jia, Z.; Zuo, W.; Han, H.; Xie, K.; Li, L. Research on the construction of novel nano-modified clean fracturing fluid and the migration characteristics of proppants. *Energy Sci. Eng.* **2024**, *12*, 5429–5442. [CrossRef]
18. Yelemessova, G.T.; Gussenov, I.S.H.; Klivenko, A.N.; Orazzhanova, L.K.; Sabitova, A.N.; Shakhvorostov, A.V.; Bardadym, Y.V.; Aseyev, V.O. Hydrophobically modified acrylamide hydrogel particles for conformance control: Synthesis, characterization and enhanced oil recovery performance. *J. Appl. Polym. Sci.* **2025**, *142*, e57900. [CrossRef]
19. Afolabi, R.O.; Oluyemi, G.F.; Officer, S.; Ugwu, J.O. Hydrophobically associating polymers for enhanced oil recovery—Part A: A review on the effects of some key reservoir conditions. *J. Pet. Sci. Eng.* **2019**, *180*, 681–698. [CrossRef]
20. Song, N.-N.; Li, M.-C.; Guo, X.-Q.; Zhang, Y.-X.; Xin, M.-Y.; Sun, J.-S.; Lv, K.-H.; Liu, C.-Z. Lignin in oilfield application: Current trends and future perspectives. *Pet. Sci.* **2025**, *22*, 4292–4315. [CrossRef]
21. Bloise, E.; Lazzoi, M.R.; Mergola, L.; Del Sole, R.; Mele, G. Advances in nanomaterials based on cashew nut shell liquid. *Nanomaterials* **2023**, *13*, 2486. [CrossRef] [PubMed]
22. Caillol, S. The future of cardanol as small giant for biobased aromatic polymers and additives. *Eur. Polym. J.* **2023**, *193*, 112096. [CrossRef]
23. Rao, H.S.P.; Kamalraj, M.; Swain, J.; Mishra, A.K. Characterization and phase transition study of a versatile molecular gel from a glucose-triazole-hydrogenated cardanol conjugate. *RSC Adv.* **2014**, *4*, 12175–12181. [CrossRef]
24. Wang, J.; Gu, F.; Han, W.; Fu, L.; Dong, S.; Zhang, Z.; Ren, Z.; Liao, K. Green surfactant made from cashew phenol for enhanced oil recovery. *ACS Omega* **2023**, *8*, 2057–2064. [CrossRef] [PubMed]
25. Meng, J.; Cai, M.; Zhu, Z.; Lin, X.; Wang, Q.; Shang, H.; Wang, L. Dynamic gel-forming properties of cardanol modified phenolic resin gel system in long snake-like simulation core with heterogeneity matching actual reservoir conditions. *Energy Sources Part A Recovery Util. Environ. Eff.* **2023**, *45*, 11207–11223. [CrossRef]
26. Tyman, J.H.P.; Bruce, I.E. Surfactant properties and biodegradation of polyethoxylates from phenolic lipids. *J. Surfactants Deterg.* **2004**, *7*, 169–173. [CrossRef]
27. Okay, O. Hydrogels: From simple covalently cross-linked systems toward hydrophobically associating adaptive semicrystalline materials. *Macromol. Mater. Eng.* **2026**, *311*, 70304. [CrossRef]
28. Ferraz, F.M.B.; Reichart, C.; Kainz, L.; Moitzi, C. DLS-derived apparent mobility as a formulation-relevant descriptor of thermoresponsive methylcellulose gelation and hysteresis. *Gels* **2026**, *12*, 766. [CrossRef] [PubMed]
29. Hopkins, C.C.; de Bruyn, J.R. Gelation and long-time relaxation of aqueous solutions of Pluronic F127. *J. Rheol.* **2019**, *63*, 191–201. [CrossRef]
30. Schild, H.G. Poly(N-isopropylacrylamide): Experiment, Theory and Application. *Prog. Polym. Sci.* **1992**, *17*, 163–249.
31. Wanka, G.; Hoffmann, H.; Ulbricht, W. Phase Diagrams and Aggregation Behavior of Poly(oxyethylene)-poly(oxypropylene)-poly(oxyethylene) Triblock Copolymers in Aqueous Solutions. *Macromolecules* **1994**.
32. Sydansk, R.D. A Newly Developed Chromium(III) Gel Technology. *SPE Reserv. Eng.* **1990**, *5*, 346–352.
33. Jeong, B.; Bae, Y.H.; Kim, S.W. Thermoreversible Gelation of PEG-PLGA-PEG Triblock Copolymer Aqueous Solutions. *Macromolecules* **1999**, *32*, 7064–7069.
34. Liu, X.; Wang, S.; Shi, W.; Liu, H. Thermo-/pH-dual-sensitive PEG/PAMAM nanogel: Reaction dynamics and plugging application of CO_2 channeling. *Gels* **2022**, *8*, 683. [CrossRef] [PubMed]
35. Macias, E.; Travesset, A. Hydrogen bond network disruption by hydration layers in water solutions with salt and hydrogen-bonding polymers (PEO). *J. Phys. Chem. B* **2023**, *127*, 6778–6794. [CrossRef] [PubMed]
36. Liang, S.; Zou, J.; Meng, L.; Fu, K.; Li, X.; Wang, Z. Impacts of high salinity on antifouling performance of hydrophilic polymer-modified reverse osmosis (RO) membrane. *J. Membr. Sci.* **2024**, *708*, 123042. [CrossRef]

37. Liu, F.; Yin, D.; Sun, J.; Luo, X.; Huang, X. Preparation and characterization of temperature-sensitive gel plugging agent. *Gels* **2024**, *10*, 742. [CrossRef] [PubMed]
38. Paroushi, M.S.; Tian, X.; Bai, B.; Schuman, T.P.; Zhang, Y.; Wei, M. Effect of ionic strength on gelation time and strength of AMPS-based polymer gels. In Proceedings of the SPE Improved Oil Recovery Conference, Tulsa, OK, USA, 21 April 2026; SPE-231529-MS.

Disclaimer/Publisher's Note: The statements, opinions and data contained in all publications are solely those of the individual author(s) and contributor(s) and not of MDPI and/or the editor(s). MDPI and/or the editor(s) disclaim responsibility for any injury to people or property resulting from any ideas, methods, instructions or products referred to in the content.